Geophysical Journal International

Geophys. J. Int. (2024) **236,** 88–98
Advance Access publication 2023 September 26
GJI Gravity, Geodesy and Tides

https://doi.org/10.1093/gji/ggad371

Combining atmospheric and non-tidal ocean loading effects to correct high precision gravity time-series

E. D. Antokoletz [1,2,3] H. Wziontek,[1] H. Dobslaw [4] K. Balidakis,[4] T. Klügel,[1] F. A. Oreiro[5] and C. N. Tocho[2]

[1]*Federal Agency for Cartography and Geodesy (BKG), 04105 Leipzig, Germany. E-mail: Ezequiel.Antokoletz@bkg.bund.de*
[2]*Facultad de Ciencias Astronómicas y Geofísicas—National University of La Plata (FCAG-UNLP), B1900FWA La Plata, Argentina*
[3]*National Scientific and Technical Research Council (CONICET), B1900FWA La Plata, Argentina*
[4]*German Research Centre for Geosciences (GFZ), Section 1.3: Earth System Modelling, 14473 Potsdam, Germany*
[5]*Servicio de Hidrografía Naval (SHN), C1270ABV Capital Federal, Argentina*

Accepted 2023 September 18. Received 2023 September 5; in original form 2023 April 24

SUMMARY

In modelling atmospheric loading effects for terrestrial gravimetry, state-of-the-art approaches take advantage of numerical weather models to account for the global 3-D distribution of air masses. Deformation effects are often computed assuming the Inverse Barometer (IB) hypothesis to be generally valid over the oceans. By a revision of the IB assumption and its consequences we show that although the seafloor is not deformed by atmospheric pressure changes, there exists a fraction of ocean mass that current modelling schemes are usually not accounting for. This causes an overestimation of the atmospheric attraction effect over oceans, even when the dynamic response of the ocean to atmospheric pressure and wind is accounted through dynamic ocean models. This signal can reach a root mean square variability of a few nm s^{-2}, depending on the location of the station. We therefore test atmospheric and non-tidal ocean loading effects at five superconducting gravimeter (SG) stations, showing that a better representation of the residual gravity variations is found when Newtonian attraction effects due to the IB response of the ocean are correctly considered. A sliding window variance analysis shows that the main reduction takes place for periods between 5 and 10 d, even for stations far away from the oceans. Since periods of non-tidal ocean mass variability closely resemble atmospheric signals recorded by SGs, we recommend to directly incorporate both an ocean component together with the IB into services that provide weather-related corrections for terrestrial gravimetry.

Key words: Geodetic instrumentation; Loading of the Earth; Time variable gravity.

1 INTRODUCTION

Due to their high sensitivity, superconducting gravimeters (SGs) are affected by mass redistribution in the atmosphere, oceans and the continental hydrosphere. Since gravity is an integrative signal affected by any possible mass change processes in the Earth's system, smaller signals can be separated and studied only by carefully modelling and removing effects with larger amplitudes. For this reason, gravity corrections have to be as accurate as possible to allow for a correct interpretation of the residual signal. Since SGs provide information for particular stations, they allow for a reliable and precise validation of mass variations represented by atmospheric, ocean and hydrological models thanks to their long-term instrumental stability and high temporal resolution, which is not affected by temporal aliasing that often complicates the analysis of satellite observations from non-geostationary orbits.

Besides Earth tides, the atmosphere is one of the most significant contributions to time-variable gravity variations, which reaches up to 10% of the signal recorded by SGs (Hinderer *et al.* 2015). Atmospheric effects for terrestrial gravimetry can be accounted for through different methodologies, such as a constant admittance factor for the local air pressure records (Torge 1989), also recognizing the frequency dependency of the admittance (e.g. Warburton & Goodkind 1977), or the use of global surface pressure fields and temperature profiles of a standard atmosphere to infer vertical air density distribution (Merriam 1992). State-of-the-art approaches take the 3-D mass distribution of the atmosphere provided by numerical weather models into account (e.g. Neumeyer *et al.* 2004; Klügel & Wziontek 2009), acknowledging that basic approaches which rely only on local air pressure records cover already 90-95% of the total effect, but do not reflect the spatial distribution of air masses around a station. From numerical weather models, attraction

and deformation components are computed separately. Newtonian attraction effects are calculated for a spatial 3-D grid of model cells up to a certain distance, whilst outside of this distance, mass variations are directly derived from atmospheric surface pressure only, which represents an accurate 2-D approximation of the atmospheric masses.

Roughly two-thirds of the Earth's surface are covered by oceans that respond dynamically to time-variable atmospheric pressure and surface winds. However, at temporal scales with periods of a few days and longer (Ponte 1994), the sea-surface adjusts to atmospheric pressure changes almost instantaneously in order to always maintain a local hydrostatic equilibrium, leading to the creation of the so-called Inverse Barometer assumption (IB; Wunsch & Stammer 1997). This assumption is often applied for the computation of atmospheric loading effects for terrestrial gravimetry (e.g. Klügel & Wziontek 2009) and implies that the oceans fully compensate atmospheric pressure variations such that no deformation occurs at the seafloor. More complex descriptions of the ocean response to atmospheric pressure and winds have been achieved through global ocean circulation models, which provide information about the time-variable water mass redistribution that can be used subsequently to calculate oceanic gravimetric attraction and deformation effects. Non-tidal ocean loading effects have been found to be relevant for the interpretation of SG data (Kroner *et al.* 2009), and thus were considered before in terrestrial gravimetry (e.g. Zerbini *et al.* 2004; Mikolaj *et al.* 2016).

Terrestrial gravimeters are typically installed at the surface of the Earth's crust which deforms in response to surface loading. In contrast to other geodetic techniques, not only gravity changes induced by vertical displacements of the sensor (free-air effect) but also attraction effects due to the redistribution of mass have to be considered. In this regard, the aim of this paper is to carefully consider the consequences of the IB response in order to consistently account for all contributions in atmospheric attraction calculations for terrestrial gravimetry, even in the case of including non-tidal ocean loading effects based on global ocean circulation models. Through this analysis, we show that state-of-the-art modelling approaches of atmospheric loading effects for terrestrial gravimetry overestimate attraction effects over oceans and, thus, services that provide such corrections should take it into account. To illustrate this, we evaluate observed gravity residuals at five SG stations against atmospheric and non-tidal ocean loading effects based on the Atmospheric attraction computation service (Atmacs; Klügel & Wziontek 2009) of the Federal Agency for Cartography and Geodesy (BKG) and the Max-Planck-Institute for Meteorology Ocean Model (MPIOM; Jungclaus *et al.* 2013), respectively. Finally, we analyse the global distribution of the overestimated effect in order to emphasize its importance for further interpretation of gravity residuals in terms of, for example, terrestrial water storage.

2 ATMOSPHERIC LOADING CALCULATIONS AND CONSEQUENCES OF THE INVERSE BAROMETER ASSUMPTION

The computation of the Newtonian attraction effects of air mass variations requires special consideration in the vicinity of the station. The application of numerical weather models (e.g. Neumeyer *et al.* 2004; Klügel & Wziontek 2009), allows for the best possible representation of the local situation benefitting from the 3-D air mass distribution around the computation point. While in case of an empirical air pressure admittance also global loading effects are implicitly included, the latter approaches require a separate consideration of deformation effects. Elastic deformation (including the indirect effect) is usually computed with Green's functions following the concept of Farrell (1972), where the mass load is derived from the surface pressure of these models assuming a hydrostatic equilibrium. Thus, the mass load ($\mathrm{d}m$) is simply obtained by

$$\mathrm{d}m = \frac{(P - P_0)\,\mathrm{d}A}{g_0}, \tag{1}$$

where P is the atmospheric surface pressure of a given column of base area $\mathrm{d}A$, P_0 is a pressure reference value and g_0 is a gravity reference value, usually in accordance with WMO (2008) and conventionally applied in numerical atmosphere and ocean models.

Over the oceans, the simplest assumption is that they respond as an IB where all atmospheric pressure changes are perfectly compensated. Consequently, some authors, for example, Klügel & Wziontek (2009) or Abe *et al.* (2010), simply define atmospheric surface pressure

$$P = \begin{cases} P & \text{over continents} \\ P_0 & \text{over oceans.} \end{cases} \tag{2}$$

Practically, mass anomalies over oceans are set to zero. Extended approaches (e.g. Boy *et al.* 2009) consider mass conservation within the oceans and set $P_0 = \bar{P} = \frac{1}{A_{\mathrm{Oc}}} \iint_{\mathrm{Oc}} P\,\mathrm{d}A$ in eq. (2). Here, $\bar{P}$ is a mean surface pressure value over the ocean area (A_{Oc}) at a given time, also called static contribution of the atmosphere to ocean-bottom pressure (Dobslaw *et al.* 2017b).

On the other hand, the Newtonian attraction contribution to gravity (g_{AN}) for a single column of air at a certain moment of time has a vertical component (Merriam 1992)

$$g_{\mathrm{AN}}(\Psi) = -G \int_0^{z_{\max}} \frac{\rho(z)\sin\alpha}{r^2}\mathrm{d}A\,\mathrm{d}z, \tag{3}$$

where Ψ is the spherical distance between the column and the computation point, z corresponds to the vertical distance within the column and ρ is the air density, while r is the vector distance between the volume element of air $\mathrm{d}A\,\mathrm{d}z$ and the computation point, and α is the angle between r and the local horizon at the computation point.

A 3-D air mass distribution was found only to be relevant up to a certain distance from the computation point (e.g. Abe *et al.* 2010). Outside of such a region, mass can be condensed to a single point mass located at or near the Earth's surface, which greatly simplifies the computation of attraction effects. In this case and assuming hydrostatic equilibrium again, the mass contribution for a given column is obtained from eq. (1) and, thus, eq. (3) can be split up into two regions where only up to a spherical distance D from the computation point the 3-D distribution of air masses is accounted for

$$g_{\mathrm{AN}}(\Psi) = -G \begin{cases} \int_0^{z_{\max}} \frac{\rho(z)\sin\alpha}{r^2}\mathrm{d}A\,\mathrm{d}z & 0 < d \le D \\ \frac{\mathrm{d}m\sin\alpha}{r^2} & d > D. \end{cases} \tag{4}$$

The total Newtonian attraction effect results then from the sum over all columns of area $\mathrm{d}A$. Consequently, this includes mass variations over oceans, in either case. Requirements on the choice of D are further discussed in Abe *et al.* (2010).

It is important to consider the impact of mass variations at the sea surface due to the IB response as illustrated with Fig. 1. An atmospheric pressure change at the sea surface induced by air mass changes of that column will be compensated by a water mass change so that the total pressure at the seafloor remains constant. In consequence, this results in a spatial redistribution of air and water

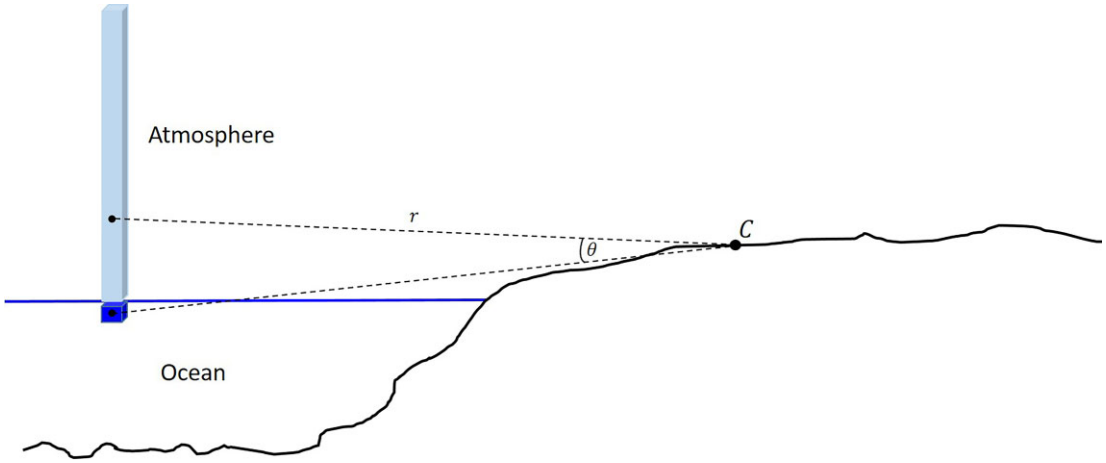

Figure 1. Schematic view of the IB response of the ocean to atmospheric pressure changes.

masses. If both components (atmosphere and ocean) are considered individually, as it is common practice, Newtonian mass attraction effects which are induced by this mass redistribution mostly compensate each other. For a distant point C where the angle θ (Fig. 1) is close to zero, their magnitudes are almost identical and thus compensate to zero.

Using numerical weather models, the atmospheric mass attraction effect is usually computed globally including the oceans. However, in some implementations, for example, Klügel & Wziontek (2009) or Mikolaj *et al.* (2016) the compensating attraction term due to the IB response of the oceans is missing and causes an overestimation of the attraction effects over oceans.

Finally, when including non-tidal ocean loading effects based on a global ocean circulation model, gravity effects are derived from ocean-bottom pressure variations (e.g. Mikolaj *et al.* 2016), which only represent the dynamic ocean response to atmospheric forcing but do not include any mass variations related to the IB (Dobslaw *et al.* 2017a). Therefore, it becomes necessary to always account for the mass attraction effect from the oceans, either in case of IB or when using an additional model for ocean dynamics. Since the mass redistribution occurs close to the sea surface, it is sufficient to apply the hydrostatic assumption eq. (1) with $P_0 = \bar{P}$, and locate it as point masses at the sea surface. This allows further to employ the 3-D atmospheric mass distribution for stations close to the coast. In addition, although no deformation of the seafloor occurs due to the IB, a complete and more precise definition should also include the ocean mass conservation by also setting $P_0 = \bar{P}$ in eq. (2).

Table 1 summarizes the total contributions from the atmosphere and the oceans for a given computation point described above as included in the state-of-the-art modelling approaches. In the case of the atmosphere, attraction and deformation effects are computed separately as the spatial distribution of air masses is important in particular in the surrounding of the station. Due to the IB response of the oceans to atmospheric pressure changes, there is an additional attraction effect that has not always been accounted for. If additionally an ocean circulation model is included, non-tidal ocean loading effects are computed based on mass anomalies usually located at the sea surface.

An alternative approach to solve the missing contribution would be to completely abandon the IB hypothesis for the computation of atmospheric effects on gravity and, consequently, the ocean response to air pressure and winds. Experiments performed with data sets presented in the next section suggest that equivalent results to those presented in this study are achieved when accounting for the total effect from the atmosphere and the oceans. Further details on this approach and its results that also underline advantages of using IB are given in the Supporting Information.

3 ATMOSPHERIC AND OCEANIC DATA SETS

Atmospheric effects were derived in this study from a global configuration of the Icosahedral Nonhydrostatic (ICON; Zängl *et al.* 2015) model framework of the German Weather Service (DWD), as provided by Atmacs. The ICON model is based on atmospheric data on a triangular grid size of about 13 km and with a temporal resolution of 3 hr, which is provided daily to BKG to compute loading effects for numerous SG stations. In Atmacs, the computation of Newtonian attraction effects is divided into a local, a regional and the remaining global part. Inside the local and regional zone, the discrete 3-D distribution of air masses around a spherical distance of 15° of the station is accounted for. Within a radius of 200 km (local zone), the resolution of the point masses is increased by a factor of 400 to account for the spatial extent of the cells and horizontal density gradients. Outside the local and regional areas, the air column is condensed to its centre of mass, at approximately 5.4 km height. Deformation effects are derived from the surface atmospheric pressure assuming the IB for the oceans as defined in eq. (2). While this causes by definition no deformation at the seafloor, the mass attraction induced by compensation of atmospheric mass changes is omitted and, therefore, atmospheric mass attraction effects are always computed globally including the oceans. In contrast, the compensating ocean mass contribution is missing. Therefore, the mass attraction effect due to the IB over oceans is mistakenly included. Consequently, the compensating water mass redistribution due to the IB has been separately computed based on surface atmospheric pressure from the mentioned model and eq. (1).

Non-tidal ocean loading effects within this study were based on ocean-bottom pressure variations from MPIOM, forced by atmospheric fields from the operational prediction model of the European Centre for Medium-Range Weather Forecasts (ECMWF; Dobslaw *et al.* 2017b). Atmospheric forcing data sets include surface atmospheric pressure, wind, temperature, cloud cover, radiation and precipitation. Global data were provided by the German Research Centre for Geosciences (GFZ) in a regular grid of 0.5° × 0.5° spacing and a temporal resolution of 3 hr. We use these inputs to derive

Table 1. Summary of atmospheric and non-tidal ocean contributions included in state-of-the-art modelling approaches for terrestrial gravimetry. The attraction component of the IB is usually implicitly ignored.

Source	Effect	Included?
Atmosphere	Attraction of air mass distribution (eq. 4)	Yes
	Deformation due to the surface mass load	Yes
Ocean	Attraction of the IB response of the ocean	**No**
	Attraction and deformation of ocean mass redistribution	Yes*

*In case of accounting for a global ocean circulation model.

mass variations using eq. (1) in order to calculate loading effects with SPOTL (Agnew 2012). All calculations were limited to the year 2018.

While we acknowledge that there exist other loading services that provide atmospheric and non-tidal ocean loading effects for terrestrial gravimetry (e.g. Boy *et al.* 2009), those selected in this study allow us to illustrate how the IB effect is considered in current atmospheric modelling schemes and how they can be complemented by an ocean dynamic model. Further comparisons with other services are subject of future work.

4 SUPERCONDUCTING GRAVITY TIME-SERIES

A set of five SG stations for year 2018 was evaluated, including: Wettzell (WE; Wziontek *et al.* 2017c) in Germany; Yebes (YS; Calvo *et al.* 2012) in Spain; Membach (MB; Van Camp *et al.* 2021) in Belgium; Medicina (MC; Wziontek *et al.* 2017b) in Italy and the Argentinean-German Geodetic Observatory (AGGO) close to the city of La Plata (LP; Wziontek *et al.* 2017a) in Argentina. Table 2 shows the location of the SG stations with their approximated distance to the coast. Fig. 2 depicts the location of the different stations.

Gravity residuals for Membach and Yebes were directly obtained from the Royal Observatory of Belgium (ROB; Van Camp *et al.* 2021) and the Level 3 data sets from the International Geodynamics and Earth Tides Service (IGETS) database (Boy *et al.* 2020), respectively. These are already reduced for Earth and ocean tides as well as polar motion and instrumental drift. Atmospheric corrections already applied during processing were restored as provided in the files and replaced by Atmacs. Due to the exchange of the atmospheric correction, small atmospheric tidal signals were notable in the gravity residuals. Those signals contained prominent amplitudes at the S1 (24 hr) and S2 (12 hr) periods, but also in its sidebands associated with seasonal modulations of the main waves (Balidakis *et al.* 2022). Since tidal variations are not in the focus of this study, high-frequency variations are suppressed by a low-pass Butterworth filter with a cut-off period of 2 d.

Besides Membach and Yebes, raw gravity measurements were considered from AGGO, Medicina and Wettzell. Pre-processing steps were applied following Hinderer *et al.* (2015). Atmospheric effects were reduced with Atmacs and polar motion effects were based on the EOP C04 14 pole coordinates series of the International Earth Rotation and Reference Systems Service using an amplitude factor of 1.16 (Wahr 1985). Earth and ocean tides were reduced by a tidal analysis performed with the ETERNA-x package, version ETA34-X-V81 (Schüller 2019a, b). As the obtained tidal models cover only waves up to monthly periods, longer periods were included based on theoretical tidal parameters (Dehant *et al.* 1999).

In the case of AGGO, local non-tidal loading effects were additionally considered based on Oreiro *et al.* (2018), where the area of the estuary of the Río de La Plata is covered (Fig. 2a). On the other hand, gravity residuals from Medicina still show tidal components related to non-stationary tidal effects (Meurers *et al.* 2016; Schroth *et al.* 2018). For this reason, the same filtering as for Membach and Yebes was also applied to this time-series.

All stations show significant seasonal variations associated with continental water storage changes. The explicit modelling of hydrological effects is rather complex because it needs the evaluation of a global model and a detailed representation of the local effects surrounding the station. As these aspects are outside the scope of this study, all gravity time-series were high-pass filtered with a Butterworth filter and a cut-off period of 150 d. Hence, seasonal signals were efficiently suppressed in order to focus on the relevant periods of non-tidal ocean loading effects at infraseasonal timescales, noting that other hydrological signals (e.g. rainfalls) may be present also in this range.

Finally, the gravity residuals for year 2018 at the five locations were compared with non-tidal ocean loading effects as well as the Newtonian attraction effects caused by ocean mass redistribution due to the IB response.

5 RESULTS AND DISCUSSION

First, the residual gravity time-series documented in Section 4 were compared with non-tidal ocean loading effects. After removal of these effects, a further comparison with the Newtonian attraction contribution due to the IB effect was performed. Secondly, the spatial distribution of the IB effect is analysed globally to identify regions where this contribution has a particularly high amplitude.

5.1 Verification of the efficiency of the loading computation by gravity time-series

Figs 3-7 depict the gravity residuals after correction of all major effects and filtering for each station together with the non-tidal ocean loading correction and the Newtonian attraction effect due to the IB response. In all cases, the upper subplot corresponds to the gravity residuals before and after removing non-tidal ocean loading effect and the IB, while the lower shows the modelled effects themselves. Step-like gravity variations visible at several stations are related to heavy rainfalls (e.g. Oreiro *et al.* 2018). Membach is an underground station and, therefore, water mass redistribution occurs mostly above the gravimeter, causing a similar behaviour but with opposite sign. For all signals, the root mean square (RMS) as an overall measure of its variability is also shown in each image.

For all stations, the modelled non-tidal ocean loading effects explain parts of the observed variability quite well. As expected, inland stations are less affected by ocean mass anomalies compared to stations at the coast, also reflected by a lower reduction of the overall RMS. Consequently, the magnitude of the loading effects is considerably lower for stations such as Wettzell or Yebes. If

Table 2. Location of the SG stations and its approximated distance to the coast.

Station	Latitude (°)	Longitude (°)	Height (m)	Coastal distance (km)
Wettzell (WE)	49.1448	12.8763	614	380
Yebes (YS)	40.5238	− 3.0902	918	260
Membach (MB)	50.6085	6.0095	250	205
Medicina (MC)	44.5248	11.6448	28	50
AGGO (LP)	− 34.8732	− 58.1400	25	15/200*

*Distance to the estuary of Río de La Plata and distance to the ocean.

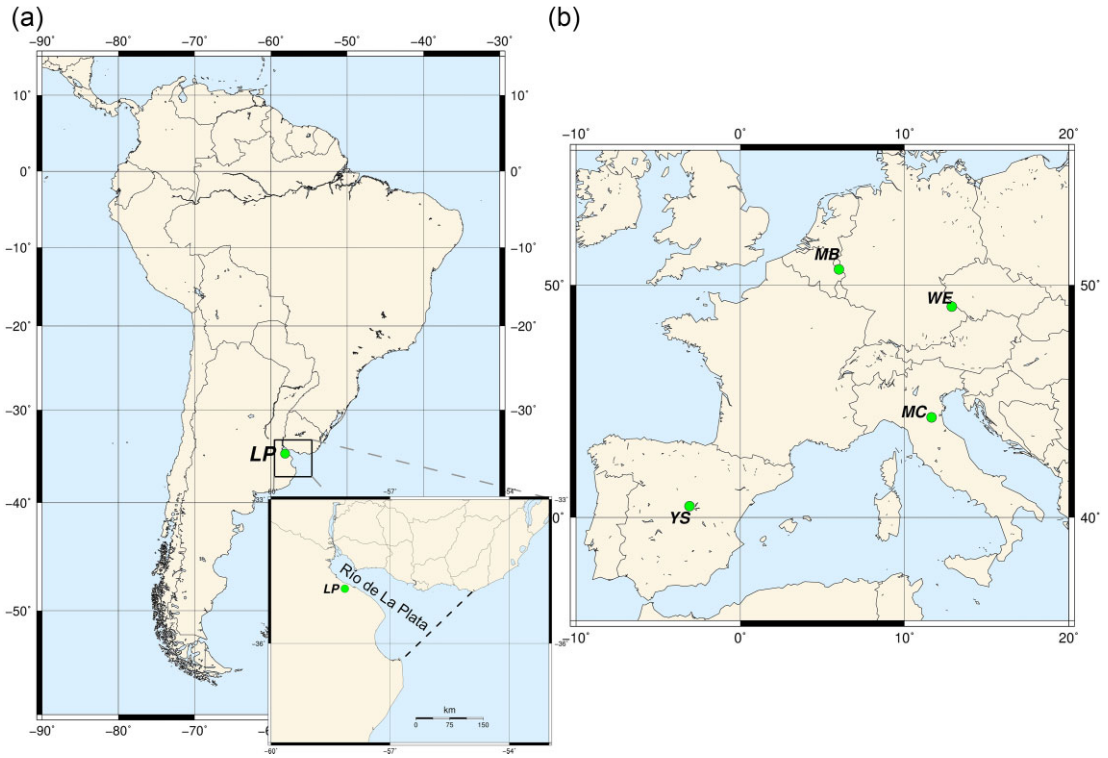

Figure 2. (a) Location of AGGO station in South America with the area of the estuary of the Río de La Plata. (b) Location of European stations.

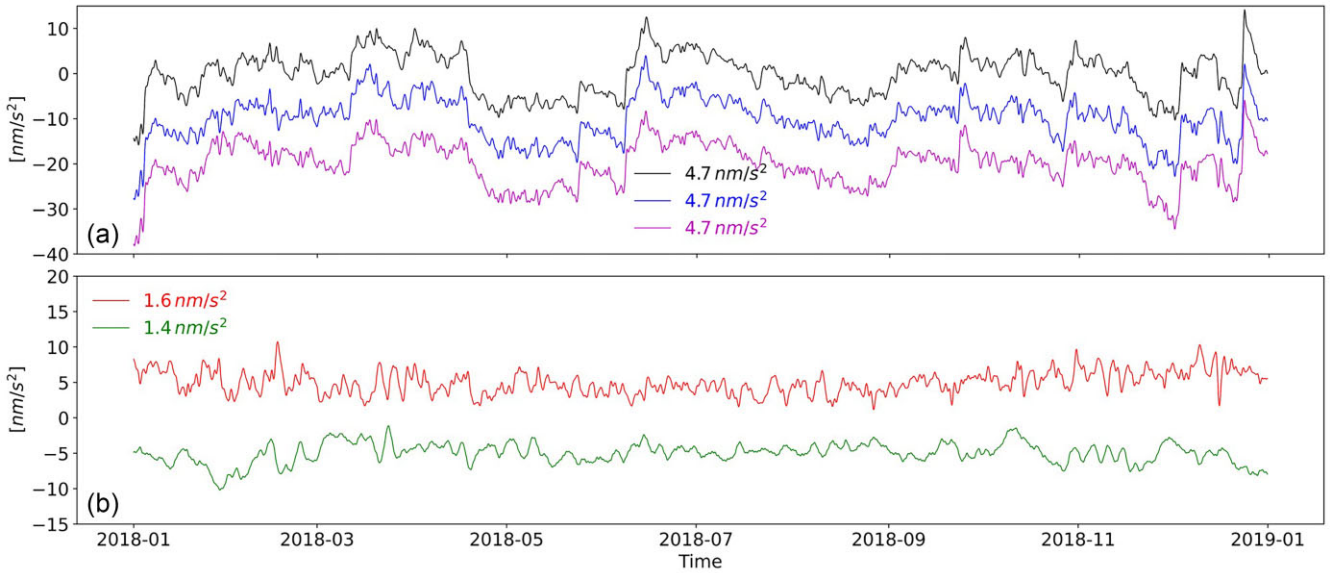

Figure 3. Station Wettzell. (a) Gravity residuals before (black), after removing non-tidal ocean loading effects (blue), and after additionally removing Newtonian attraction due to the IB response (magenta). (b) Non-tidal ocean loading effects (red) and the Newtonian attraction due to the IB response (green). Offsets were arbitrarily applied. The RMS is included for each signal.

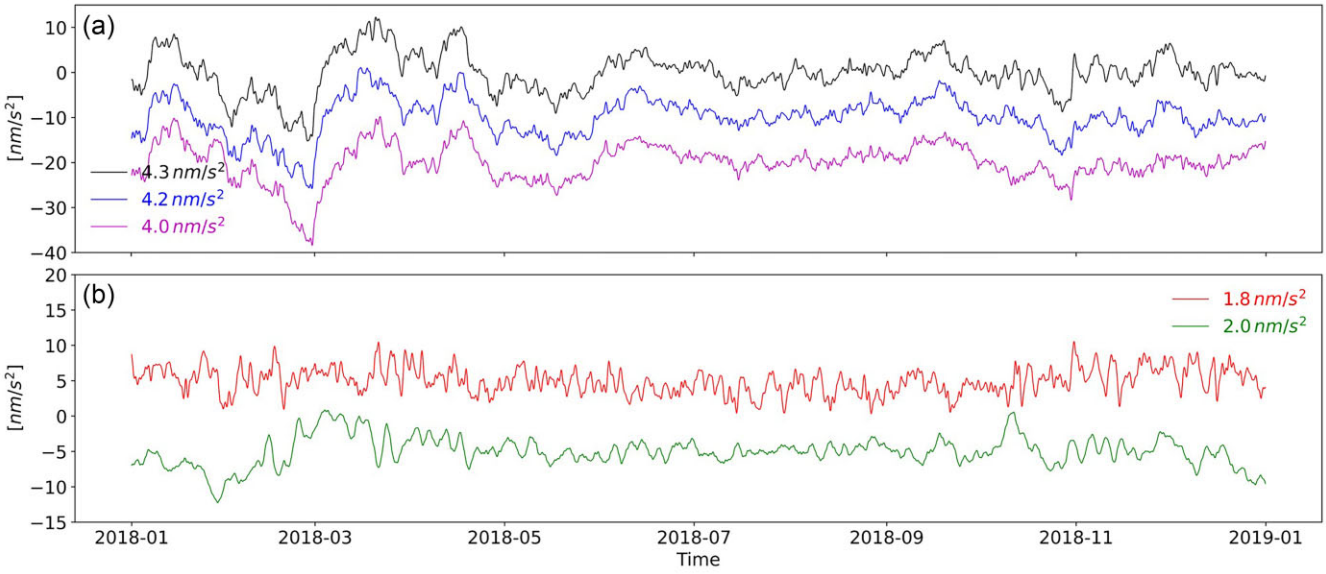

Figure 4. Station Yebes. (a) Gravity residuals before (black), after removing non-tidal ocean loading effects (blue), and after additionally removing Newtonian attraction due to the IB response (magenta). (b) Non-tidal ocean loading effects (red) and the Newtonian attraction due to the IB response (green). Offsets were arbitrarily applied. The RMS is included for each signal.

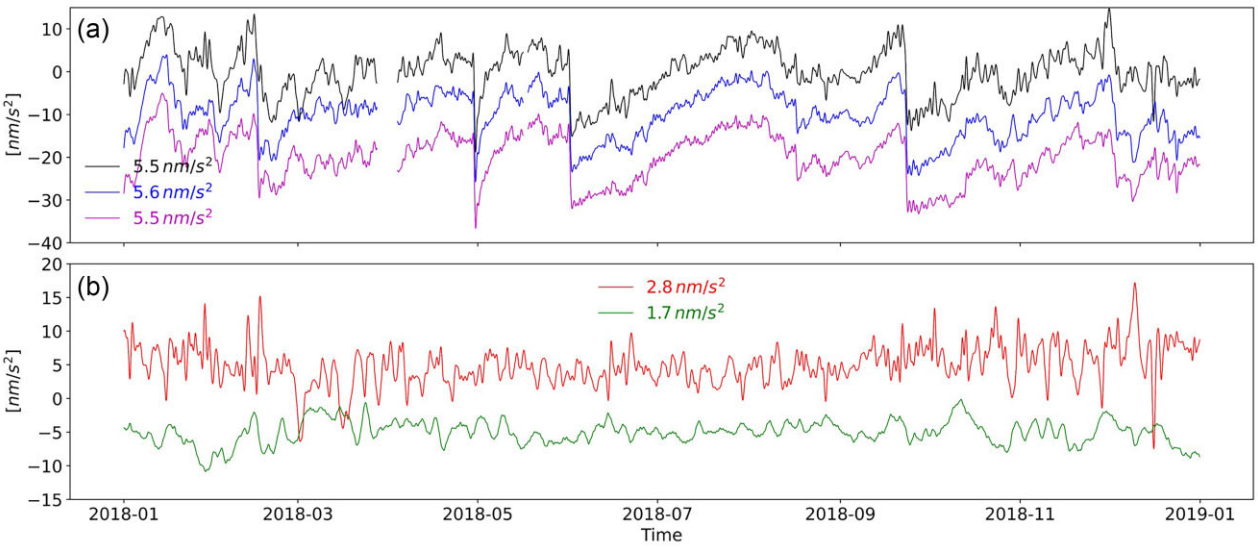

Figure 5. Station Membach. (a) Gravity residuals before (black), after removing non-tidal ocean loading effects (blue), and after additionally removing Newtonian attraction due to the IB response (magenta). (b) Non-tidal ocean loading effects (red) and the Newtonian attraction due to the IB response (green). Offsets were arbitrarily applied. The RMS is included for each signal.

a station is located closer to the coast like Medicina or AGGO, the effect becomes more relevant. Nevertheless, the overall picture shows that loading effects based on MPIOM explains the observed gravity variations and, therefore, would further reduce its variability.

Once the non-tidal ocean loading effect is removed from the gravity residuals, we compare the remaining signal with the attraction effect related to the IB response. It is notable that for all stations, this effect further explains part of the remaining variability of the gravity residuals. In particular for specific periods, for example, between 2018 October and November for station Wettzell or at the beginning of 2018 December for station Yebes, the computed effect follows almost perfectly the residual signal from the SGs. A similar behaviour can be observed between 2018 June and August for station Membach.

Apart from the seasonal variations associated with water storage changes which are attenuated due to filtering, gravity residuals still show significant variations related to short-term hydrological events (e.g. rain or snow-melt) that are more prominent than the effects under consideration in this paper. For this reason and in order to analyse the capability of each correction to reduce the variability of the gravity residuals at the target periods of this study, a sliding window variance analysis was performed. Different period bands and a set of Butterworth bandpass filters were selected using windows having a length of 90 d and being shifted by 15 d. The gravity residuals before and after removing the non-tidal ocean and IB corrections were analysed for comparison.

Fig. 8 depicts the results for the five selected stations. The winter season (i.e. June–September in the Southern Hemisphere and

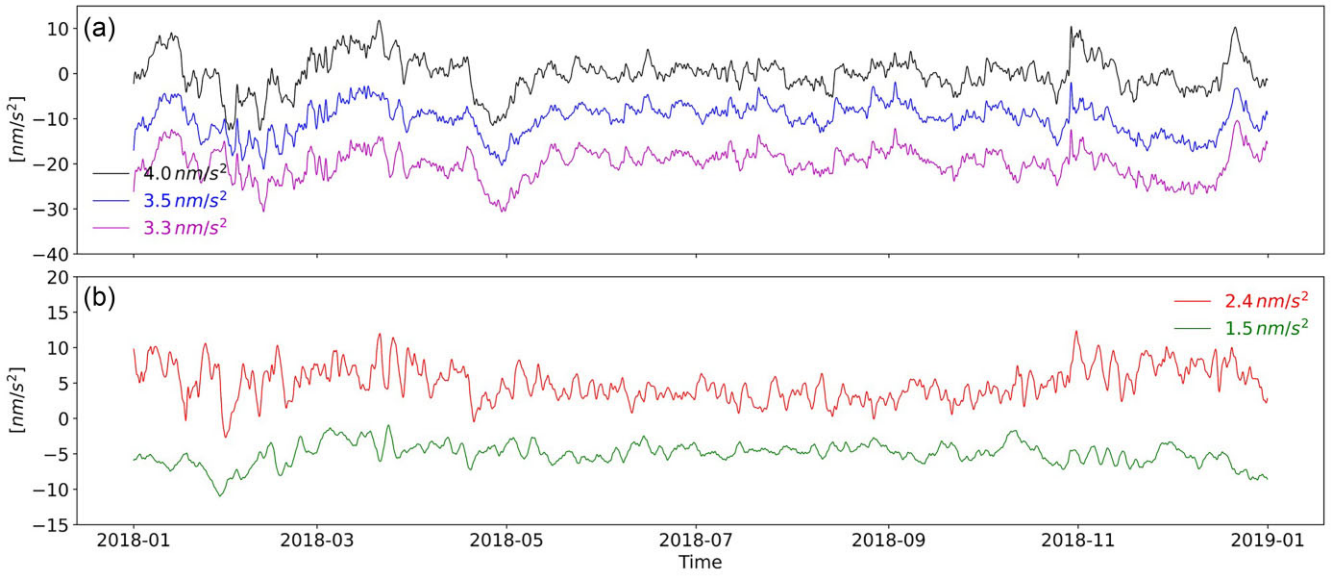

Figure 6. Station Medicina. (a) Gravity residuals before (black), after removing non-tidal ocean loading effects (blue), and after additionally removing Newtonian attraction due to the IB response (magenta). (b) Non-tidal ocean loading effects (red) and the Newtonian attraction due to the IB response (green). Offsets were arbitrarily applied. The RMS is included for each signal.

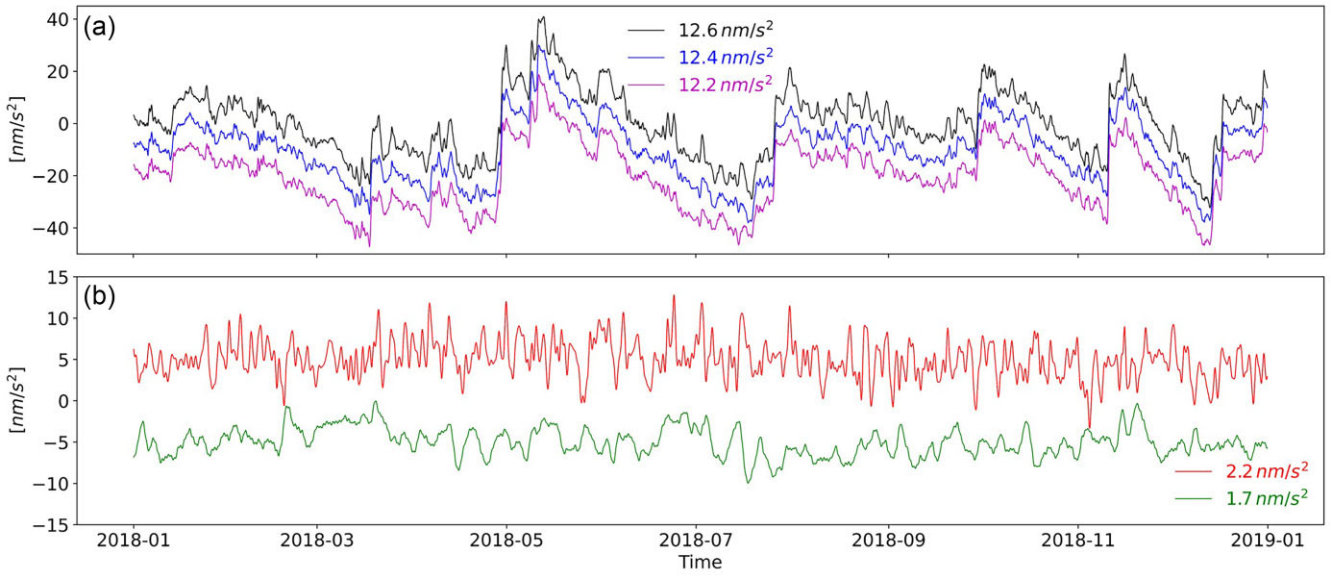

Figure 7. Station AGGO. (a) Gravity residuals before (black), after removing non-tidal ocean loading effects (blue), and after additionally removing Newtonian attraction due to the IB response (magenta). (b) Non-tidal ocean loading effects (red) and the Newtonian attraction due to the IB response (green). Offsets were arbitrarily applied. The RMS is included for each signal.

December–March in the Northern Hemisphere) shows the largest variability of the signal related to enhanced ocean dynamics (e.g. stronger storm surge effects and a seasonally more vivid ocean circulation). Therefore, all European stations show a common larger variability at the beginning of the year, reflecting that these stations are dominated by common mass variations. As expected, the non-tidal ocean loading correction reduces the variance of the gravity residuals at certain periods in particular. For all stations, up to 30% of the signal is explained for periods between 3–7 d, reaching up to 40–45% for periods between 10 and 15 d. A notable variance reduction of 30–35% was found for longer periods up to 30 d for stations Yebes, Membach and Medicina.

Moreover, accounting for the Newtonian attraction of the IB response properly allows to further reduce the variability, as revealed by the third column of Fig. 8. For periods from 3 to 6 d, the percentage of reduction reaches only 5%, suggesting that there are only small contributions from this effect at these frequencies. However, significant reductions up to 20% were found for periods between 7 and 10 d in all time-series. For periods around 15 d, Medicina and AGGO show reductions up to 15%, while the other stations show this reduction for longer periods up to 30 d. Overall, while the Newtonian attraction of the IB response is a small contribution reflected also by its variance in the fourth column, it further explains the gravity residuals at several periods.

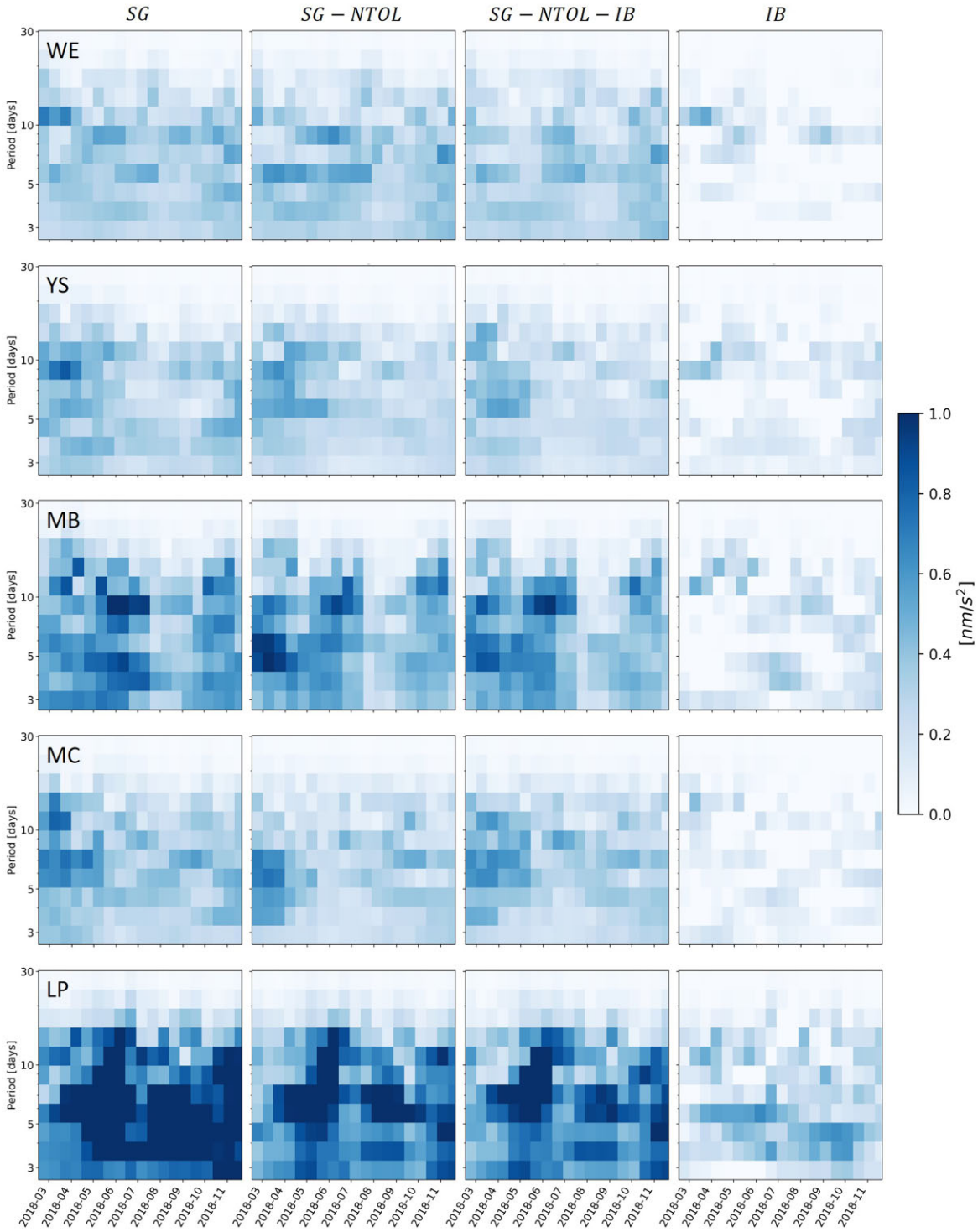

Figure 8. Sliding window variance analysis for each station along the year 2018. The first column corresponds to the gravity residuals before applying non-tidal ocean and IB corrections (SG). The second column corresponds to the gravity residuals corrected for non-tidal ocean loading effects (SG − NTOL), while in the third, the correction for the IB effect is also applied (SG − NTOL − IB). The fourth column shows the variance of the IB effect (*IB*).

Due to the fact that AGGO (LP) is the closest station to the coast considered, it shows the largest variability in the range from 5 to 10 d, which is not completely removed after applying both corrections, especially between April and June. This can either be explained by the presence of signals from other sources (e.g. hydrology) at those periods, or by the complex setting of ocean dynamics at the Argentine shelf and within the Rio de La Plata estuary, which are not well reproduced in MPIOM.

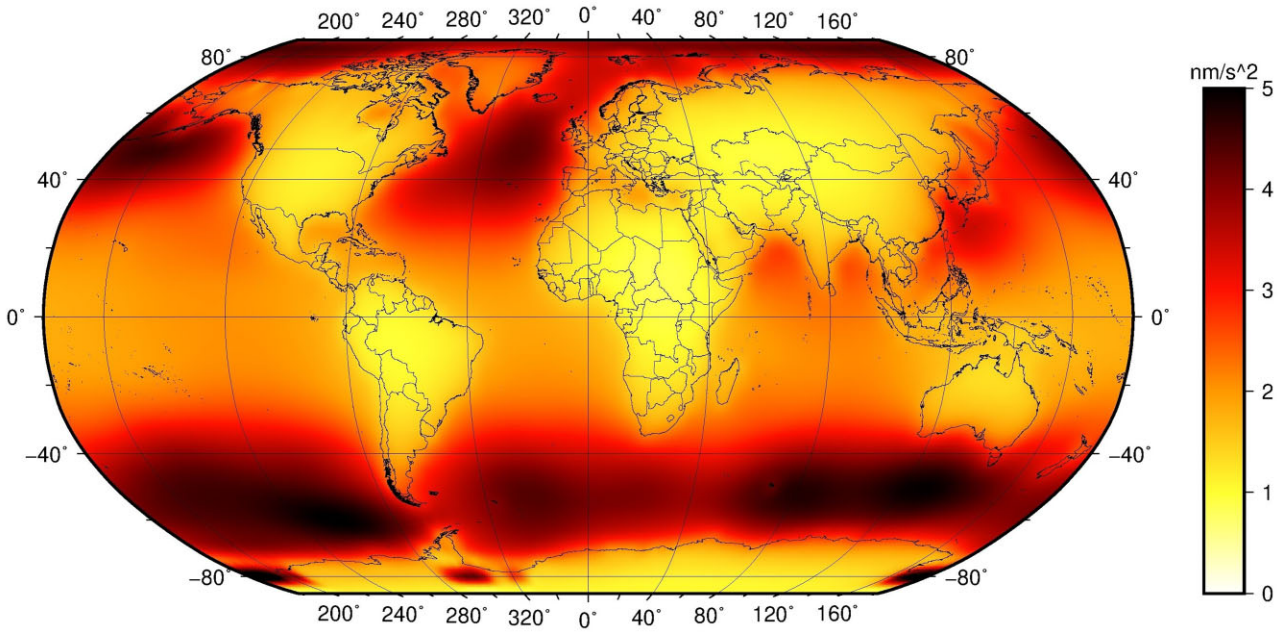

Figure 9. RMS global distribution of the Newtonian attraction effect due to the IB response of the ocean to atmospheric pressure changes.

5.2 Spatial distribution of the IB effect

Properly incorporating the Newtonian attraction effect due to the IB response of the ocean to atmospheric pressure changes allows to further reduce the variability of the gravity residuals at the five analysed stations. This effect can reach an RMS up to a few nm s^{-2}, depending on the location of the station with respect to the coast. The largest amplitude is observed at station Yebes (260 km from the Atlantic coast) with an RMS of 2 nm s^{-2}. This suggests that even when the station is located far from the coast, this effect can be large enough if the station is surrounded by oceans with strong bottom pressure variability. For station Wettzell, which has the largest distance to a coast from all stations considered (almost 400 km, see Table 2), non-tidal ocean loading effects have a minor impact but the IB effect shows an RMS of 1.4 nm s^{-2}. This is still significant for a further interpretation of the residuals, for example, in terms of water storage variations (e.g. Creutzfeldt *et al.* 2010; Hector *et al.* 2013; Fores *et al.* 2019; Watlet *et al.* 2020).

The amplitude of the IB effect was analysed globally for the year 2018, evaluated on a grid having a $5^\circ \times 5^\circ$ spatial resolution. Fig. 9 shows the RMS of the effect. We observe that the largest variability is seen along the Antarctic Circumpolar Current (ACC), the North Atlantic, the Bering Sea, the Philippine Sea and the Arctic Ocean, suggesting that if a station is located in these regions and close to the coast (e.g. the Patagonia region in South America, East Asia, Iceland or Greenland), this effect becomes larger. At continental stations, the RMS still amounts to a few nm s^{-2} which is significant for many applications of SG observations in Earth system science.

6 CONCLUSIONS

Even small contributions from atmosphere and oceans are relevant in the analysis of high precision terrestrial gravity time-series. It has been shown that in up-to-date modelling approaches of atmospheric effects, the Newtonian attraction component due to the IB assumption is missing. This causes an overestimation of the total atmospheric effect over the oceans, which is also not covered when including non-tidal ocean loading effects based on ocean-bottom pressure products.

To illustrate the impact of this missing contribution, terrestrial gravity time-series have been evaluated at five stations with varying distance to the coast. Residual gravity variations as measured by SGs are corrected for atmospheric loading effects taken from the Atmacs, and then compared with non-tidal ocean loading effects based on ocean-bottom pressure data from an ocean simulation with the MPIOM forced by atmospheric data sets of the operational prediction model of the ECMWF. The results are well supported by the gravity residuals. Larger reductions are found, especially for stations close to the coast or more exposed to ocean mass variations. Once these non-tidal ocean loading effects are removed from the observed signal, a further reduction of the variability of the residuals can be achieved when considering the Newtonian attraction effects due to the IB response of the ocean to atmospheric pressure changes. It confirms that this contribution which is usually missing in many modelling approaches is significant. Because the effects are non-stationary, a sliding window variance analysis was performed to further visualize the performance of both corrections for different period bands and seasons. It turned out that non-tidal ocean loading effects efficiently reduce the signal variability of the gravity residuals for periods ranging from 3 to 30 d, reaching up to 45% of reduction for periods between 10 and 15 d. By considering the IB contribution, further reduction is found, especially for periods from 7 to 10 d, where it allows for a reduction of 20% of the residual variability. Coastal stations also showed reductions up to 15% for periods around 15 d.

The IB correction for the five selected stations shows RMS variations up to a few nm s^{-2}. This correction was also analysed globally, demonstrating that for coastal stations such variations can be even larger. Significant deviations are found in areas such as Southern Patagonia, East Asia, or Iceland, showing the importance of including this effect when modelling atmospheric loading effects for terrestrial gravimetry. Work will therefore be continued towards integrating non-tidal ocean mass effects directly into computation services like Atmacs in order to facilitate users with state-of-the-art

correction models for near-surface mass variability. Accurate signal separation products as provided by Atmacs are crucial for various objectives in terrestrial gravimetry where long-standing observations are essential, like the identification of Slichter Modes indicative of the Dynamics of the Core (Ding & Chao 2015) or the monitoring of geothermal activity (Schäfer *et al.* 2020). Moreover, the accurate removal of transient atmospheric and oceanic signals are critically important for the isolation of hydrological signals in terrestrial gravimeter recordings (Güntner *et al.* 2017), so that correction services such as Atmacs will certainly play a critical role in developing gravimetry into an essential tool to quantify long-term changes in water availability at both global and regional scales (Güntner *et al.* 2023).

SUPPORTING INFORMATION

Supplementary data are available at *GJI* online.

suppl_data

Please note: Oxford University Press is not responsible for the content or functionality of any supporting materials supplied by the authors. Any queries (other than missing material) should be directed to the corresponding author for the paper.

ACKNOWLEDGMENTS

The authors sincerely thank the editor, Prof Duncan Agnew, and the anonymous reviewers for their supportive comments and suggestions during the review process of this paper. The authors also acknowledge Michael Van Camp from the ROB for providing the gravity time-series for Membach station, IGETS for providing Level 3 data for station Yebes and all stations operators for the maintenance of the different SGs used in this study. KB is funded by the DFG via the Collaborative Research Cluster TerraQ (SFB 1464, project-ID 434617780). EA, HW, HD, TK and FO worked on the numerical modelling. EA and HW processed the time-series of SGs. HD and KB provided expertise on ocean and atmospheric data sets used in this study. FO provided the local non-tidal ocean loading effects for the estuary of the Río de La Plata. EA, HW, HD and CT drafted and coordinated the work on the manuscript. All authors contributed on the final version of the manuscript.

DATA AVAILABILITY

Gravity time-series are available through the database of the IGETS: http://isdc.gfz-potsdam.de/igets-data-base/. Atmospheric corrections used in this study are available through the Atmacs: http://atmacs.bkg.bund.de/. Geodetic data products based on MPIOM global ocean simulations are publicly available from GFZ's Information System and Data Center (https://doi.org/10.5880/GFZ.1.3.2022.003).

REFERENCES

Abe, M., Kroner, C., Neumeyer, J. & Chen, X., 2010. Assessment of atmospheric reductions for terrestrial gravity observations, *Bull. Inform. des Marées Terr.,* **146,** 11817–11838. https://www.eas.slu.edu/GGP/BIM_Recent_Issues/bim146-2010/abe_etal_atmospheric_gravity_reductions_bim146_10.pdf

Agnew, D.C., 2012. SPOTL: some programs for ocean-tide loading, Scripps Institution of Oceanography, UC San Diego. Retrieved from https://escholarship.org/uc/item/954322pg.

Balidakis, K., Sulzbach, R., Shihora, L., Dahle, C., Dill, R. & Dobslaw, H., 2022. Atmospheric contributions to global ocean tides for satellite gravimetry, *J. Adv. Model. Earth Syst.,* **14**(11), e2022MS003193 , doi:10.1029/2022MS003193.

Boy, J.-P., Barriot, J.-P., Förste, C., Voigt, C. & Wziontek, H., 2020. *Achievements of the First 4 years of the International Geodynamics and Earth Tide Service (IGETS) 2015–2019,* pp. 1–6, Springer, Berlin, Heidelberg.

Boy, J.-P., Longuevergne, L., Boudin, F., Jacob, T., Lyard, F., Llubes, M., Florsch, N. & Esnoult, M.-F., 2009. Modelling atmospheric and induced non-tidal oceanic loading contributions to surface gravity and tilt measurements, *J. Geodynam.,* **48**(3), 182–188

Calvo, M., Córdoba, B., Serna, J., Rosat, S. & López, J., 2012. Presentation of the new Spanish Gravimeter Station; Yebes, in *EGU General Assembly Conference Abstracts,* p. 12006. https://ui.adsabs.harvard.edu/abs/2012EGUGA..1412006C.

Creutzfeldt, B., Güntner, A., Wziontek, H. & Merz, B., 2010. Reducing local hydrology from high-precision gravity measurements: a lysimeter-based approach, *Geophys. J. Int.,* **183**(1), 178–187.

Dehant, V., Defraigne, P. & Wahr, J., 1999. Tides for a convective Earth, *J. geophys. Res.: Solid Earth,* **104**(B1), 1035–1058.

Ding, H. & Chao, B.F., 2015. The slichter mode of the earth: revisit with optimal stacking and autoregressive methods on full superconducting gravimeter data set, *J. geophys. Res.: Solid Earth,* **120**(10), 7261–7272.

Dobslaw, H. *et al.*, 2017b. A new high-resolution model of non-tidal atmosphere and ocean mass variability for de-aliasing of satellite gravity observations: AOD1B RL06, *Geophys. J. Int.,* **211**(1), 263–269.

Dobslaw, H., Bergmann-Wolf, I., Dill, R., Poropat, L. & Flechtner, F., 2017a. GRACE 327-750 - Gravity Recovery and Climate Experiment Product Description Document for AOD1B Release 06 (Rev. 6.1, October 19, 2017). https://gfzpublic.gfz-potsdam.de/pubman/item/item_5006868.

Farrell, W., 1972. Deformation of the Earth by surface loads, *Rev. Geophys.,* **10**(3), 761–797.

Fores, B., Klein, G., Le Moigne, N. & Francis, O., 2019. Long-term stability of tilt-controlled gphonex gravimeters, *J. geophys. Res.: Solid Earth,* **124**(11), 12264–12276.

Güntner, A. *et al.*, 2023. Veränderungen der Wasserspeicherung in Deutschland seit 2002 aus Beobachtungen der Satellitengravimetrie, *Hydrol. Wasserbewirtschaft.,* **67**(2), 74–89.

Güntner, A., Reich, M., Mikolaj, M., Creutzfeldt, B., Schroeder, S. & Wziontek, H., 2017. Landscape-scale water balance monitoring with an iGrav superconducting gravimeter in a field enclosure, *Hydrol. Earth Syst. Sci.,* **21**(6), 3167–3182.

Hector, B. *et al.*, 2013. Gravity effect of water storage changes in a weathered hard-rock aquifer in West Africa: results from joint absolute gravity, hydrological monitoring and geophysical prospection, *Geophys. J. Int.,* **194**(2), 737–750.

Hinderer, J., Crossley, D. & Warburton, R., 2015. Superconducting Gravimetry, *Treatise on Geophysics,* **Vol. 3,** 2nd edn, pp. 59–115.

Jungclaus, J. *et al.*, 2013. Characteristics of the ocean simulations in the Max Planck Institute Ocean Model (MPIOM) the ocean component of the MPI-Earth system model, *J. Adv. Model. Earth Syst.,* **5**(2), 422–446.

Klügel, T. & Wziontek, H., 2009. Correcting gravimeters and tiltmeters for atmospheric mass attraction using operational weather models, *J. Geodynam.,* **48**(3), 204–210.

Kroner, C., Thomas, M., Dobslaw, H., Abe, M. & Weise, A., 2009. Seasonal effects of non-tidal oceanic mass shifts in observations with superconducting gravimeters, *J. Geodynam.,* **48**(3), 354–359.

Merriam, J.B., 1992. Atmospheric pressure and gravity, *Geophys. J. Int.,* **109**(3), 488–500.

Meurers, B., Van Camp, M., Francis, O. & Pálinkáš, V., 2016. Temporal variation of tidal parameters in superconducting gravimeter time-series, *Geophys. J. Int.,* **205**(1), 284–300.

Mikolaj, M., Meurers, B. & Güntner, A., 2016. Modelling of global mass effects in hydrology, atmosphere and oceans on surface gravity, *Comput. Geosci.,* **93,** 12–20.

Neumeyer, J., Hagedoorn, J., Leitloff, J. & Schmidt, T., 2004. Gravity reduction with three-dimensional atmospheric pressure data for precise ground gravity measurements, *J. Geodynam.,* **38**(3), 437–450.

Oreiro, F., Wziontek, H., Fiore, M., D'Onofrio, E. & Brunini, C., 2018. Non-tidal ocean loading correction for the Argentinean-German Geodetic Observatory using an empirical model of storm surge for the Río de la Plata, *Pure appl. Geophys.,* **175**(5), 1739–1753.

Ponte, R.M., 1994. Understanding the relation between wind-and pressure-driven sea level variability, *J. geophys. Res.: Oceans,* **99**(C4), 8033–8039.

Schäfer, F. *et al.*, 2020. Performance of three iGrav superconducting gravity meters before and after transport to remote monitoring sites, *Geophys. J. Int.,* **223**(2), 959–972.

Schroth, E., Forbriger, T. & Westerhaus, M., 2018. *A Catalogue of Gravimetric Factor and Phase Variations for Twelve Wave Groups,* Karlsruher Institut für Technologie (KIT).

Schüller, K., 2019a. *Installation Guide. Manual-03-ETA34-X-V71-Installation-Guide*. Surin, https://eterna.bkg.bund.de/eterna/index.html%3Fp=4693.html#Eterna.

Schüller, K., 2019b. *User's Guide. Manual-02-ET34-ANA-V71*.Surin, https://eterna.bkg.bund.de/.

Torge, W., 1989. *Gravimetry,* De Gruyter, Berlin, Boston.

Van Camp, M., Hendrickx, M., Castelein, S. & Martin, H., 2021. Superconducting gravimeter data from Membach, *GFZ Data Services*. doi: 10.5880/igets.mb.l1.001.

Wahr, J.M., 1985. Deformation induced by polar motion, *J. geophys. Res.: Solid Earth,* **90**(B11), 9363–9368.

Warburton, R.J. & Goodkind, J.M., 1977. The influence of barometric-pressure variations on gravity, *Geophys. J. Int.,* **48**(3), 281–292.

Watlet, A., Van Camp, M., Francis, O., Poulain, A., Rochez, G., Hallet, V., Quinif, Y. & Kaufmann, O., 2020. Gravity monitoring of underground flash flood events to study their impact on groundwater recharge and the distribution of karst voids, *Water Resour. Res.,* **56**(4), e2019WR026673.

WMO, 2008. *Guide to Meteorological Instruments and Methods of Observation (WMO-No. 8),* World Meteorological Organisation Geneva, Switzerland

Wunsch, C. & Stammer, D., 1997. Atmospheric loading and the oceanic 'inverted barometer' effect, *Rev. Geophys.,* **35**(1), 79–107.

Wziontek, H., Wolf, P., Häfner, M., Hase, H., Nowak, I., Rülke, A., Wilmes, H. & Brunini, C., 2017a. Superconducting gravimeter data from AGGO/La Plata - Level 1, *GFZ Data Services*.

Wziontek, H., Wolf, P., Nowak, I., Richter, B., Rülke, A., Schwahn, W., Wilmes, H. & Zerbini, S., 2017b. Superconducting gravimeter data from Medicina - Level 1, *GFZ Data Services*. doi: 10.5880/igets.mc.l1.001.

Wziontek, H., Wolf, P., Nowak, I., Richter, B., Rülke, A. & Wilmes, H., 2017c. Superconducting gravimeter data from Wettzell - Level 1, *GFZ Data Services*. doi: 10.5880/igets.we.l1.001.

Zängl, G., Reinert, D., Rípodas, P. & Baldauf, M., 2015. The ICON (ICOsahedral Non-hydrostatic) modelling framework of DWD and MPI-M: description of the non-hydrostatic dynamical core, *Q. J. R. Meteorol. Soc.,* **141**(687), 563–579.

Zerbini, S., Matonti, F., Raicich, F., Richter, B. & van Dam, T., 2004. Observing and assessing nontidal ocean loading using ocean, continuous GPS and gravity data in the Adriatic area, *Geophys. Res. Lett.,* **31**(23). doi: 10.1029/2004GL021185.